

Elliptic flow of hadrons in equal-velocity quark combination mechanism in relativistic heavy-ion collisions

Jun Song,¹ Hai-hong Li,¹ and Feng-lan Shao^{2,*}

¹*Department of Physics, Jining University, Shandong 273155, China*

²*School of Physics and Physical Engineering, Qufu Normal University, Shandong 273165, China*

We apply a quark combination model with equal-velocity combination (EVC) approximation to study the elliptic flow (v_2) of hadrons in heavy-ion collisions in a wide collision energy range ($\sqrt{s_{NN}} = 27 - 5020$ GeV). Utilizing the simple relationship between v_2 of hadrons and those of quarks under EVC, we find that v_2 of up/down quarks obtained by experimental data of proton is consistent with that obtained by data of Λ and Ξ . v_2 of strange quarks obtained by data of Ω is consistent with that obtained by data of Λ and Ξ , and at RHIC energies it is also consistent with that obtained by data of ϕ . This means that v_2 of these hadrons have a common quark-level source. Using data of D^0 , we obtain v_2 of charm quarks with $p_T \lesssim 6$ GeV/c. We find that under EVC charm quark dominates v_2 of D mesons at low p_T but light-flavor quarks significantly contribute to v_2 of D mesons in the range $3 \lesssim p_T \lesssim 8$ GeV/c. We predict v_2 of charmed baryons Λ_c^+ and Ξ_c^0 which show a significant enhancement at intermediate p_T due to the double contribution of light-flavor quarks. The properties of the obtained quark v_2 under EVC are studied and a regularity for v_2 of quarks as the function of p_T/m is found.

I. INTRODUCTION

In non-central heavy-ion collisions, momentum distributions of the produced hadrons are anisotropic in the transverse plane perpendicular to the beam direction [1]. The elliptic flow (v_2) is the second harmonic coefficient of Fourier expansion for the azimuthal distribution of particle transverse momentum and denotes the asymmetry between x and y components of particle transverse momentum. v_2 of hadron carries important information on the degree of initial thermalization, the pressure gradients, the equation of state, and the hadronization for the created quark matter [1–5].

In non-central heavy-ion collisions at RHIC and LHC energies, the data of v_2 for light-flavor hadrons as the function of transverse momentum (p_T) exhibit a number-of-constituent quark scaling (NCQ) property [5–9]. As v_2 and p_T of identified hadrons are divided by the number of constituent quarks (2 for meson, 3 for baryon), the scaled data of different hadrons approximately follow a common tendency. Replacing p_T by the transverse kinetic energy $KET = \sqrt{p_T^2 + m^2} - m$ in the horizontal axis, NCQ looks better. Such a NCQ is expected in quark recombination/coalescence model [10–17]. The preliminary data of D^0 in Au+Au collisions at $\sqrt{s_{NN}} = 200$ GeV [18] seemingly also follow this NCQ.

In our recent works, we found a constituent quark number scaling property exhibited in the p_T spectra of identified hadrons in high multiplicity pp , p -Pb and AA collisions [19–21]. This property is the direct consequence of the equal-velocity combination (EVC) of constituent quarks and antiquarks at hadronization. We further demonstrated that EVC can self-consistently explain the data of p_T spectra for different identified hadrons in

high multiplicity pp and p -Pb collisions at LHC energies [20, 22–24] and in heavy-ion collisions in a wide collision energy range [25]. Taking advantage of rich data for hadronic v_2 in heavy-ion collisions, in particular, at RHIC BES energies [6–8, 26, 27], it is interesting to further study whether this EVC mechanism works for v_2 of hadrons or not.

Because of different constituent mass such as $m_d \approx m_u \approx 0.3$ GeV, $m_s \approx 0.5$ GeV and $m_c = 1.5$ GeV, quarks of different flavors under EVC will contribute different momenta (proportional to quark mass) to the formed hadron. Therefore, $p_T/2$ for meson and $p_T/3$ for baryon in the aforementioned NCQ operation on v_2 data of light-flavor hadrons can not exactly denote the transverse momentum of each quark in the hadron containing different quark flavors. Instead, we should divide the momentum of hadron into different pieces so as to obtain the actual momentum of the quark at hadronization and the actual relationship between quark transverse momentum and its v_2 . Therefore, applying the EVC to study hadronic v_2 data will bring new results for v_2 of quarks at hadronization.

In this paper, we apply the quark combination model (QCM) with EVC to systematically study the v_2 of identified hadrons and extract the v_2 of quarks at hadronization using the available data of identified hadrons in heavy-ion collisions in a wide collision energy range ($\sqrt{s_{NN}} = 27\text{GeV} - 5.02\text{TeV}$) [6–8, 26, 27]. We distinguish at first the v_2 of strange quarks from that of up/down quarks. We extract them separately from the data of different hadrons and study the consistency of results from different extraction channels as the test of EVC mechanism. With the obtained v_2 of light-flavor quarks, we further obtain the v_2 of charm quarks from the data of D^0 . We study the dominant ingredient for v_2 of D mesons at different p_T and predict v_2 of charmed baryons Λ_c^+ and Ξ_c^0 . Finally, we discuss the properties for the extracted v_2 of up/down, strange and charm quarks.

* shao@mail.sdu.edu.cn

The paper is organized as follows. In Sec. II, we derive the v_2 of hadrons in QCM with EVC. In Sec. III and Sec. IV, we apply formulas of EVC to decompose the data of hadron v_2 at RHIC and LHC energies into v_2 of up/down quarks and that of strange quarks at hadronization. We study the consistency for results obtained from different extraction channels. In Sec. V, we study the v_2 of charm quarks extracted from D^0 data at LHC and RHIC energies. In Sec. VI, we study properties of the extracted v_2 of quarks. The summary and outlook are given at last.

II. HADRONIC v_2 IN QCM WITH EVC

In this section, we apply a quark combination model with equal-velocity combination (EVC) approximation [19, 22] to study the production of identified hadrons in the two-dimension transverse plane at mid-rapidity. Here, we define the distribution function $f_h(p_T, \varphi) \equiv dN_h/dp_T d\varphi$ where φ is the azimuthal angle. The distribution function of hadron under EVC is simply the product of those of quarks and/or antiquarks, i.e.,

$$f_{M_i}(p_T, \varphi) = \kappa_{M_i} f_{q_1}(x_1 p_T, \varphi) f_{\bar{q}_2}(x_2 p_T, \varphi), \quad (1)$$

$$f_{B_i}(p_T, \varphi) = \kappa_{B_i} f_{q_1}(x_1 p_T, \varphi) f_{q_2}(x_2 p_T, \varphi) f_{q_3}(x_3 p_T, \varphi). \quad (2)$$

Under EVC, the quark and/or antiquark have the same direction (φ) as the hadron and take a given fraction of p_T of the hadron. Because of $p_i = m_i \gamma v \propto m_i$ at equal velocity, the momentum fraction $x_{1,2} = m_{1,2}/(m_1 + m_2)$ for meson with $x_1 + x_2 = 1$, and $x_{1,2,3} = m_{1,2,3}/(m_1 + m_2 + m_3)$ for baryon with $x_1 + x_2 + x_3 = 1$. m_i is the constituent mass of quark q_i . κ_{M_i} and κ_{B_i} are coefficients independent of p_T and φ but can be depen-

dent on the hadron species and system size. Their expressions can be found in [22] and are not shown here since κ_{M_i} and κ_{B_i} are irrelevant to the derivation of v_2 .

The quark distribution function can be written in the following form

$$f_q(p_T, \varphi) = f_q(p_T) \left[1 + 2 \sum_{n=1}^{\infty} v_{n,q}(p_T) \cos n\varphi \right], \quad (3)$$

where we denote $f_q(p_T) \equiv dN_q/dp_T$ as the φ -independent p_T distribution function. The φ dependence part is expressed as usual in terms of the Fourier series and the harmonic coefficient is defined as

$$v_{n,q}(p_T) = \frac{\int f_q(p_T, \varphi) \cos n\varphi d\varphi}{\int f_q(p_T, \varphi) d\varphi}. \quad (4)$$

In this paper, we study the second harmonic coefficient v_2 of hadrons. Using Eqs. (1)-(3), we obtain for meson $M_i(q_1 \bar{q}_2)$

$$\begin{aligned} v_{2,M_i}(p_T) &= \frac{\int d\varphi \cos 2\varphi f_{M_i}(p_T, \varphi)}{\int d\varphi f_{M_i}(p_T, \varphi)} \\ &= \frac{1}{\mathcal{N}_{M_i}} \left[v_{2,q_1} + v_{2,\bar{q}_2} \right. \\ &\quad \left. + \sum_{n,m=1}^{\infty} v_{n,q_1} v_{m,\bar{q}_2} (\delta_{2,m+n} + \delta_{n,2+m} + \delta_{m,2+n}) \right] \end{aligned} \quad (5)$$

with

$$\mathcal{N}_{M_i} = 1 + 2 \sum_{n=1}^{\infty} v_{n,q_1} v_{n,\bar{q}_2}. \quad (6)$$

Here, we use the abbreviation v_{2,q_1} for $v_{2,q_1}(x_1 p_T)$ and v_{2,\bar{q}_2} for $v_{2,\bar{q}_2}(x_2 p_T)$. For baryon $B_i(q_1 q_2 q_3)$, we have

$$\begin{aligned} v_{2,B_i}(p_T) &= \frac{1}{\mathcal{N}_{B_i}} \left\{ v_{2,q_1} + v_{2,q_2} + v_{2,q_3} + \sum_{n,m=1}^{\infty} (v_{n,q_1} v_{m,q_2} + v_{n,q_1} v_{m,q_3} + v_{n,q_2} v_{m,q_3}) (\delta_{m,n+2} + \delta_{n,m+2} + \delta_{m+n,2}) \right. \\ &\quad \left. + \sum_{n,m,k=1}^{\infty} v_{n,q_1} v_{m,q_2} v_{k,q_3} (\delta_{k,m+n+2} + \delta_{k,m+n-2} + \delta_{n,k+m-2} + \delta_{n,k+m+2} + \delta_{m,k+n-2} + \delta_{m,k+n+2}) \right\} \end{aligned} \quad (7)$$

with

$$\mathcal{N}_{B_i} = 1 + 2 \sum_{n=1}^{\infty} (v_{n,q_1} v_{n,q_2} + v_{n,q_1} v_{n,q_3} + v_{n,q_2} v_{n,q_3}) + 2 \sum_{n,m,k=1}^{\infty} v_{n,q_1} v_{m,q_2} v_{k,q_3} (\delta_{k,m+n} + \delta_{n,k+m} + \delta_{m,k+n}), \quad (8)$$

where we use the abbreviation v_{2,q_j} for $v_{2,q_j}(x_j p_T)$ with $j = 1, 2, 3$.

Since the data of hadronic v_1 at mid-rapidity [28, 29]

are only about $v_{1,h} \lesssim 10^{-3}$, v_1 of quarks should be very small and therefore can be safely neglected. In addition, according to NCQ estimation of the 2-4th flow of quarks

$v_{2/3/4,q} \sim 10^{-2}$ [5–9], we can neglect the influence of high order terms $(v_{n,q})^{2,3}$ in \mathcal{N}_{M_i} and \mathcal{N}_{B_i} , and obtain

$$\begin{aligned} v_{2,M_i}(p_T) &\approx v_{2,q_1} \left(1 + \sum_{n=2}^{\infty} \frac{v_{n,q_1}}{v_{2,q_1}} v_{n+2,\bar{q}_2} \right) \\ &+ v_{2,\bar{q}_2} \left(1 + \sum_{n=2}^{\infty} \frac{v_{n,\bar{q}_2}}{v_{2,\bar{q}_2}} v_{n+2,q_1} \right), \end{aligned} \quad (9)$$

and

$$\begin{aligned} v_{2,B_i}(p_T) &\approx v_{2,q_1} \left[1 + \sum_{n=2}^{\infty} \frac{v_{n,q_1}}{v_{2,q_1}} (v_{n+2,q_2} + v_{n+2,q_3}) \right] \\ &+ v_{2,q_2} \left[1 + \sum_{n=2}^{\infty} \frac{v_{n,q_2}}{v_{2,q_2}} (v_{n+2,q_1} + v_{n+2,q_3}) \right] \\ &+ v_{2,q_3} \left[1 + \sum_{n=2}^{\infty} \frac{v_{n,q_3}}{v_{2,q_3}} (v_{n+2,q_1} + v_{n+2,q_2}) \right]. \end{aligned} \quad (10)$$

Here we split the v_2 of meson into two parts and that of baryon into three parts. Each part is v_2 of constituent quark multiplying a term containing the small correction from higher-order harmonic flows.

The magnitude of the correction is a few percentages because of $v_{4,q} \sim 10^{-2}$ as mentioned above [5–9]. Higher-order harmonic flows are often unavailable at present and their influence is usually expected to be not larger than these lower-order harmonic flows. In addition, the difference among $v_{n,q}$ of different quark flavors is usually much (about one order of magnitude) lower than absolute value of $v_{n,q}$. Therefore, the relative difference among terms in brackets in Eq. (9) and that among these in Eq. (10) should be very small ($\lesssim 10^{-2}$). Eqs.(9) and (10) can be thus expressed approximately as the simplest form

$$v_{2,M_i}(p_T) = v_{2,q_1}(x_1 p_T) + v_{2,\bar{q}_2}(x_2 p_T), \quad (11)$$

$$v_{2,B_i}(p_T) = v_{2,q_1}(x_1 p_T) + v_{2,q_2}(x_2 p_T) + v_{2,q_3}(x_3 p_T). \quad (12)$$

III. QUARK v_2 AT RHIC

In this section, we apply the EVC model to study the data of hadronic v_2 in heavy-ion collisions at RHIC energies. Here, we focus on proton, Λ , Ξ , Ω , and ϕ . These hadrons can be properly explained by constituent quark model with constituent masses $m_u = m_d \approx 0.3 - 0.33$ GeV and $m_s \approx 0.5 - 0.55$ GeV. Therefore, their production can be suitably described by EVC of constituent quarks at hadronization. However, pion and kaon, because of their significantly small masses, can not be directly described in the same way. We discuss their production in A.

Using Eqs. (11) and (12), we obtain

$$v_{2,\Omega}(p_T) = 3v_{2,s}(p_T/3), \quad (13)$$

$$v_{2,p}(p_T) = 3v_{2,u}(p_T/3), \quad (14)$$

$$v_{2,\phi}(p_T) = v_{2,s}(p_T/2) + v_{2,\bar{s}}(p_T/2), \quad (15)$$

$$v_{2,\Lambda}(p_T) = 2v_{2,u} \left(\frac{1}{2+r} p_T \right) + v_{2,s} \left(\frac{r}{2+r} p_T \right), \quad (16)$$

$$v_{2,\Xi}(p_T) = v_{2,u} \left(\frac{1}{1+2r} p_T \right) + 2v_{2,s} \left(\frac{r}{1+2r} p_T \right) \quad (17)$$

with the factor $r = m_s/m_u = 1.667$. Here, we use $v_{2,u} = v_{2,d}$.

We can reversely obtain v_2 of u quarks from proton or that from hyperons

$$v_{2,u}(p_T) = \frac{1}{3} v_{2,p}(3p_T), \quad (18)$$

$$v_{2,u}(p_T) = \frac{1}{3} [2v_{2,\Lambda}((2+r)p_T) - v_{2,\Xi}((1+2r)p_T)]. \quad (19)$$

We can obtain v_2 of s quarks from ϕ or hyperons

$$v_{2,s}(p_T) = \frac{1}{3} v_{2,\Omega}(3p_T), \quad (20)$$

$$v_{2,s}(p_T) = \frac{1}{2} v_{2,\phi}(2p_T), \quad (21)$$

$$v_{2,s}(p_T) = \frac{1}{3} \left[2v_{2,\Xi} \left(\frac{1+2r}{r} p_T \right) - v_{2,\Lambda} \left(\frac{2+r}{r} p_T \right) \right]. \quad (22)$$

Here, we use $v_{2,s} = v_{2,\bar{s}}$ in Eq. (21).

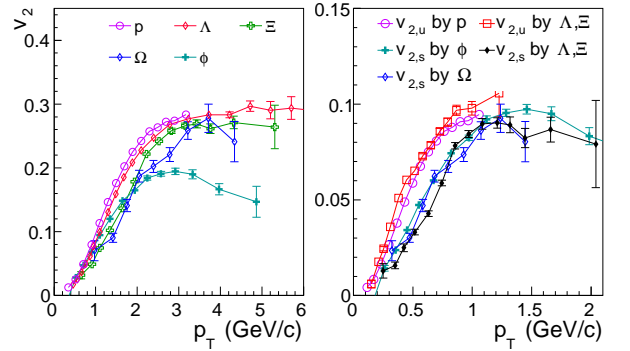


Figure 1. (a) Data for v_2 of identified hadrons at midrapidity in Au+Au collisions at $\sqrt{s_{NN}}=200$ GeV for 30-80% centrality [6]; (b) $v_{2,u}(p_T)$ and $v_{2,s}(p_T)$ extracted from these hadrons.

As an example, we first test Eqs. (18-22) by experimental data of proton, Λ ($\Lambda + \bar{\Lambda}$), Ξ ($\Xi^- + \bar{\Xi}^+$), Ω ($\Omega^- + \bar{\Omega}^+$), and ϕ in Au+Au collisions at $\sqrt{s_{NN}}=200$ GeV for 30-80% centrality [6]. Data of proton, Λ , and Ξ usually contain the decay contribution of heavier resonances. Because of decay kinematics, the influence of resonance decays on v_2 of these baryons is generally small. Therefore, we neglect this influence and directly apply

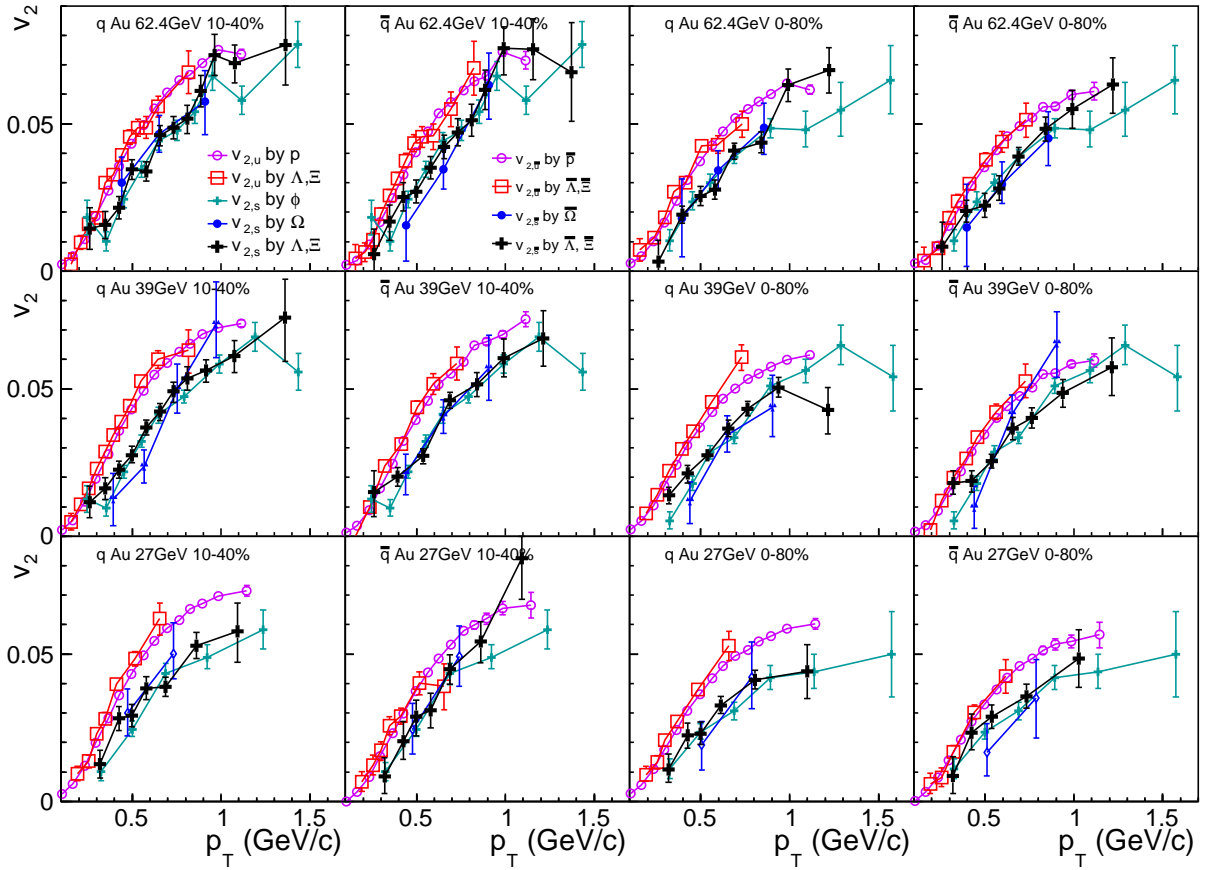


Figure 2. $v_{2,u}(p_T)$ and $v_{2,s}(p_T)$ extracted from data of identified hadrons in Au+Au collisions in different centralities and at different collision energies [26].

Eqs. (18-22) to these hadrons. We also neglect the possible rescattering effect in hadronic stage for the moment until we find its necessity in following analysis such as in ϕ study at LHC energies in next section IV.

Panel (a) in Fig. 1 shows the original data for v_2 of these hadrons which are different for different hadron species. Panel (b) shows the extracted $v_{2,u}(p_T)$ and $v_{2,s}(p_T)$ according to Eqs. (18-22). We see that $v_{2,s}(p_T)$ extracted from Ω using Eq. (20) is very close to that from ϕ using Eq. (21) and is also very close to that from Λ and Ξ data using Eq. (22). For u quarks, we see that $v_{2,u}(p_T)$ extracted from proton data using Eq. (18) is very close to that from Λ and Ξ data using Eq. (19). Therefore, v_2 data of these hadrons can be reasonably attributed to a common $v_{2,u}(p_T)$ and a common $v_{2,s}(p_T)$ at hadronization within the experimental uncertainties. In addition, we see that the extracted $v_{2,u}(p_T)$ is obviously larger than the extracted $v_{2,s}(p_T)$ in the available range $p_T \lesssim 1.2$ GeV/c, suggesting a flavor hierarchy property at quark level.

Furthermore, in Fig. 2, we carry out a systematic analysis for STAR BES data in Au+Au collisions at $\sqrt{s_{NN}} = 62.4, 39$ and 27 GeV [26]. Because experimental data at lower collision energies cover smaller p_T range and have relatively poor statistics, their results are not shown in

this paper. Here, data of hadrons and those of anti-hadrons are separately analyzed to obtain $v_{2,u}(p_T)$ and $v_{2,\bar{u}}(p_T)$. In the figure, $v_{2,s}(p_T)$ obtained by ϕ using Eq. (21) is compared with those obtained from baryons and also with those from anti-baryons. At these three collision energies each with two centralities, we see that $v_{2,u}(p_T)$ obtained from p and that from Λ and Ξ are consistent with each other. The same case is for $v_{2,\bar{u}}(p_T)$. Compared with $v_{2,u}(p_T)$ and $v_{2,\bar{u}}(p_T)$ data, $v_{2,s}(p_T)$ obtained from different strange hadrons are limited by finite statistics but are also close to each other.

IV. QUARK v_2 AT LHC AND ϕ SPECIFICITY

We further study the property of v_2 under EVC by experimental data in Pb+Pb collisions at LHC energies. In Fig. 3, we present $v_{2,u}(p_T)$ and $v_{2,s}(p_T)$ extracted from midrapidity data of proton, Λ , Ξ and Ω in Pb+Pb collisions at $\sqrt{s_{NN}} = 2.76$ and 5.02 TeV [8, 27]. We see that $v_{2,u}(p_T)$ extracted from proton and that from Λ and Ξ are very consistent. $v_{2,s}(p_T)$ extracted from Ω and that from Λ and Ξ are also very close to each other.

We further consider the ϕ data [7, 26, 27] to extract $v_{2,s}(p_T)$ and compare with those obtained from strange

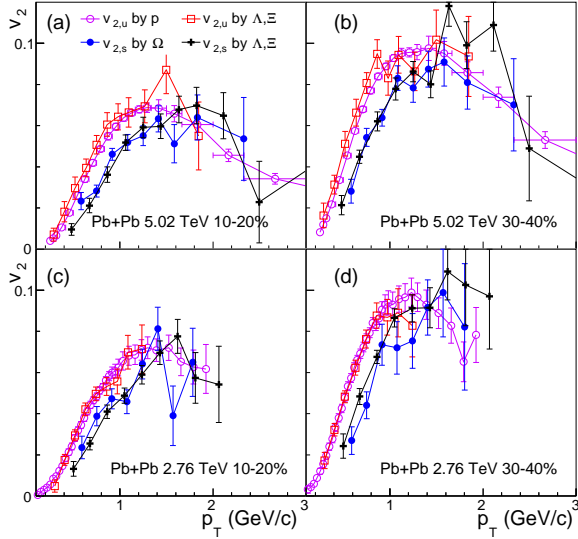


Figure 3. $v_{2,u}(p_T)$ and $v_{2,s}(p_T)$ extracted from experimental data for v_2 of identified hadrons at midrapidity in Pb+Pb collisions at LHC energies [8, 27].

baryons. The results are shown in top panels in Fig. 4. Surprisingly, even though statistical uncertainties are relatively large, we see that the $v_{2,s}(p_T)$ extracted from ϕ seems to be higher than those from strange baryons to a certain extent as $p_{T,s} \gtrsim 1$ GeV/c. This is different from the case at RHIC energies in Figs. 1 and 2.

Results in top panels in Fig. 4 imply that ϕ may receive the contribution of other production channels in heavy-ion collisions at LHC energies. Here, we consider a possible contribution, that is, two-kaon coalescence $KK \rightarrow \phi$ in hadron scattering stage [30–32]. In this case, the distribution of final-state ϕ has two contributions

$$f_{\phi}^{(final)}(p_T, \varphi) = f_{\phi, s\bar{s}}(p_T, \varphi) + f_{\phi, KK}(p_T, \varphi). \quad (23)$$

The elliptic flow is

$$v_{2,\phi}^{(final)}(p_T) = (1-z)v_{2,s\bar{s}}(p_T) + zv_{2, KK}(p_T) \quad (24)$$

with the fraction

$$z = \frac{f_{\phi, KK}(p_T)}{f_{\phi, s\bar{s}}(p_T) + f_{\phi, KK}(p_T)}. \quad (25)$$

Using the relation Eq. (15) for $s\bar{s}$ combination and the similar one for the coalescence of two kaons also with equal velocity (because the mass $m_{\phi} \approx 2m_K$), the elliptic flow of ϕ after considering the possible two-kaon coalescence has

$$v_{2,\phi}^{(final)}(p_T) \approx 2 \left[(1-z)v_{2,s} \left(\frac{p_T}{2} \right) + zv_{2,K} \left(\frac{p_T}{2} \right) \right]. \quad (26)$$

Here, we have taken $v_{2,\bar{s}} = v_{2,s}$ at LHC energies.

In bottom panels in Fig. 4, we calculate the elliptic flow of ϕ and compare with experimental data [7, 26, 27].

We firstly calculate the elliptic flow of pure $s\bar{s}$ combination. The results, marked as $s\bar{s}$ coal, are shown as the dashed lines in bottom panels in Fig. 4. The actual $v_{2,s}(p_T)$ at hadronization is identified as that by fitting data of strange baryons, see the dashed lines in top panels in Fig. 4. We see that pure $s\bar{s}$ combination can describe ϕ data in low p_T range ($p_T \lesssim 2.5$ GeV/c) but under-estimates the v_2 of ϕ at intermediate p_T ($p_T \gtrsim 2.5$ GeV/c). We then consider the contribution of two-kaon coalescence in a simple case that a p_T -independent z is taken. Using data of elliptic flow for kaons [7, 8], we calculate the elliptic flow of final-state ϕ by Eq. (26) and compare with the data. We find that data of ϕ at $p_T \gtrsim 2.5$ GeV/c at two LHC energies can be roughly described by $z = 0.2$, see solid lines in bottom panels in Fig. 4. This implies that there is about 20% of ϕ with $p_T \gtrsim 2.5$ GeV/c coming from two-kaon coalescence in the hadronic stage. We note that, compared with pure $s\bar{s}$ combination, two-kaon coalescence does not significantly increase elliptic flow of ϕ in low p_T range ($p_T \lesssim 2$ GeV/c) because here v_2 of participant kaons is small as $p_{T,K} = p_T/2 \lesssim 1$ GeV/c. Therefore, we emphasize that v_2 data of ϕ in the low p_T range do not necessarily contain the contribution of two-kaon coalescence. In addition, we note that two-kaon coalescence will influence slightly the p_T distribution function of ϕ and thus will slightly influence the quark number scaling property for p_T spectra of Ω and ϕ [19–21]. This influence is discussed in B.

V. CHARM QUARK v_2 FROM D MESONS

The EVC can be applied not only to light-flavor quarks but also to heavy-flavor quarks at hadronization [33]. In [23, 24, 34], we show the EVC of charm quarks and soft light-flavor quarks provides good description for p_T spectra of single-charm hadrons in high energy collisions. Applying EVC to elliptic flows of $D^{0,\pm}$ mesons, we obtain

$$v_{2,D}(p_T) = v_{2,u} \left(\frac{1}{1+r_{cu}} p_T \right) + v_{2,c} \left(\frac{r_{cu}}{1+r_{cu}} p_T \right) \quad (27)$$

with $r_{cu} = m_c/m_u = 5$. Since we have obtained $v_{2,u}$ in the previous sections, v_2 of charm quarks can be reversely extracted by the data of D mesons,

$$v_{2,c}(p_T) = v_{2,D} \left(\frac{1+r_{cu}}{r_{cu}} p_T \right) - v_{2,u} \left(\frac{1}{r_{cu}} p_T \right). \quad (28)$$

We note that this extraction is only valid in the low p_T range where the combination dominates D meson production. In previous studies [23, 24], we found that experimental data for p_T spectra of single-charmed hadrons in the range $p_T \lesssim 8$ GeV/c in pp and pPb collisions at LHC energies are well described by the EVC model. Therefore, experimental data of v_2 for D mesons with $p_T \lesssim 8$ GeV/c can be used to extract v_2 of charm quarks with $p_T \lesssim 6$ GeV/c in EVC model. At larger p_T , fragmentation mechanism becomes important [16, 35] and Eq. (28) is no longer valid.

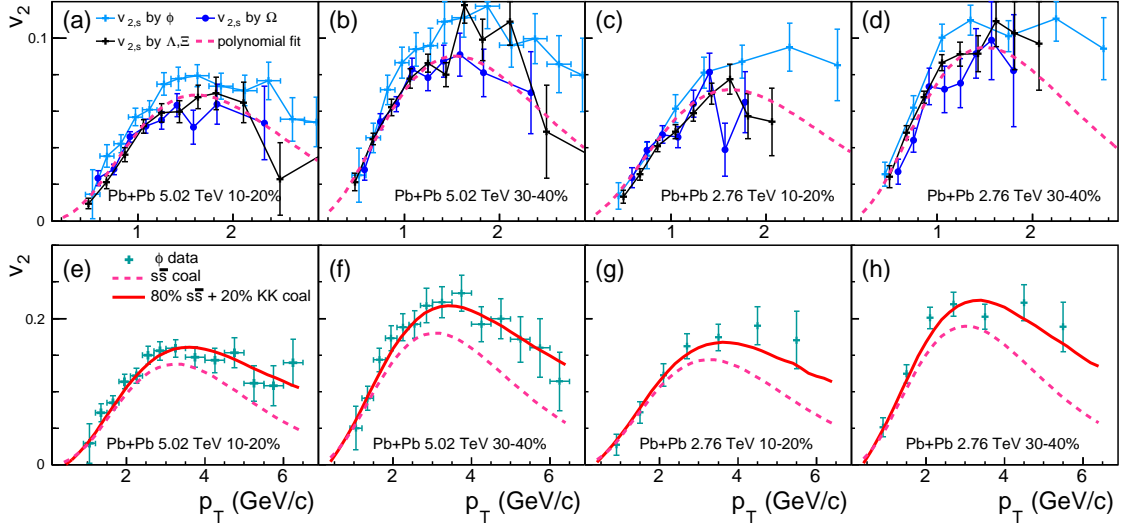


Figure 4. Top panels: $v_{2,s}(p_T)$ extracted from data of strange hadrons [7, 26, 27]. The dashed lines are polynomial fits of $v_{2,s}(p_T)$ from strange baryons. Bottom panels: The v_2 of ϕ . Symbols are data of ϕ [7, 26, 27]. The dashed lines, marked as $s\bar{s}$ coal, are results of strange quark antiquark combination. The solid lines are results considering the mixture of quark combination and two-kaon coalescence. See text for details.

In Fig. 5(a), we show the extracted $v_{2,c}(p_T)$ in Pb+Pb collisions at $\sqrt{s_{NN}} = 5.02$ TeV for 30-50% centrality. Solid circles and squares are results for $v_{2,c}(p_T)$ extracted from latest preliminary and previously published data of D^0 [36, 37], respectively. Data of D^0 are also presented in the figure as open circles and squares, respectively. The contribution of up quarks to the v_2 of D^0 at different p_T is shown as the dashed line. Under EVC, v_2 of D^0 at a specific p_T absorbs the contribution of u quark at a much smaller momentum $p_{T,u}/(1+r_{cu})$. Therefore, v_2 of D^0 in the low p_T range ($p_T \lesssim 3$ GeV/c) only receives the small contribution of u quark with $p_{T,u} \lesssim 0.5$ GeV/c, see Fig. 3. However, v_2 of D^0 in $5 \lesssim p_T \lesssim 8$ GeV/c contains the large contribution of u quark with $p_{T,u} \gtrsim 0.9$ GeV/c which is about 0.1 reading from Fig. 3. Subtracting the u quark contribution from D^0 , v_2 of charm quarks is obtained as the solid circles and squares in Fig. 5 (a). A smooth fit of these discrete points of charm quarks is shown as the solid line. We see that the v_2 of charm quarks is close to that of D^0 as $p_T \lesssim 2$ GeV/c and is smaller than the latter as $3 \lesssim p_T \lesssim 6$ GeV/c.

As $v_{2,c}$, $v_{2,u}$ and $v_{2,s}$ are obtained, we can predict v_2 of D_s^+ , Λ_c^+ and Ξ_c^0 ,

$$v_{2,D_s}(p_T) = v_{2,s}\left(\frac{1}{1+r_{cs}}p_T\right) + v_{2,c}\left(\frac{r_{cs}}{1+r_{cs}}p_T\right), \quad (29)$$

$$v_{2,\Lambda_c}(p_T) = 2v_{2,u}\left(\frac{1}{2+r_{cu}}p_T\right) + v_{2,c}\left(\frac{r_{cu}}{2+r_{cu}}p_T\right), \quad (30)$$

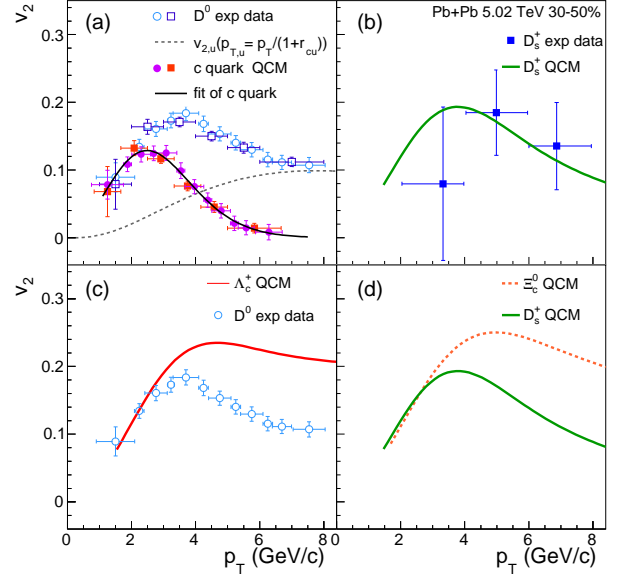


Figure 5. (a) Charm quark v_2 extracted from D^0 meson in Pb+Pb collisions at $\sqrt{s_{NN}} = 5.02$ TeV for 30-50% centrality, and (b-d) the predictions for D_s^+ , Λ_c^+ and Ξ_c^0 . Data of D^0 and D_s^+ are taken from Ref. [36–38].

$$v_{2,\Xi_c}(p_T) = v_{2,u}\left(\frac{1}{1+r+r_{cu}}p_T\right) + v_{2,s}\left(\frac{r}{1+r+r_{cu}}p_T\right) + v_{2,c}\left(\frac{r_{cu}}{1+r+r_{cu}}p_T\right) \quad (31)$$

with $r_{cs} = m_c/m_s = 3$. Here, we neglect the statistical uncertainties of the extracted datum points for v_2 of quarks and use their smooth fits, i.e., the solid line for $v_{2,c}(p_T)$ in Fig. 5 (a) and the dashed line for $v_{2,s}(p_T)$

in Fig 4(b), to calculate v_2 of D_s^+ , Λ_c^+ and Ξ_c^0 by Eqs. (29)-(31). Results are shown in Fig. 5 (b)-(d) as different types of lines.

Result of D_s^+ is compared with the preliminary data of ALICE collaboration [38]. Results of Λ_c^+ and Ξ_c^0 are compared with those of D_0 and D_s^+ . We see that v_2 of charmed baryons are close to those of charmed mesons as $p_T \lesssim 3$ GeV/c because the contribution of light-flavor quarks is very small there. As $p_T \gtrsim 4$ GeV/c, we see a significant enhancement for v_2 of charmed baryons compared with those of charmed mesons. This is because single-charm baryons absorb the v_2 of two light-flavor quarks at hadronization, see Eqs. (30) and (31), and the contribution of light-flavor quarks becomes large as $p_T \gtrsim 4$ GeV/c, e.g., see the dashed line in Fig. 5 (a) for the case of charmed mesons.

In Fig. 6 (a), we also study v_2 of charm quarks in Au+Au collisions at $\sqrt{s_{NN}} = 200$ GeV for 0-80% centrality. The result is similar to that in Pb+Pb collisions at $\sqrt{s_{NN}} = 5.02$ TeV. In the range of $p_T \lesssim 3$ GeV/c, charm quark dominates the v_2 of D^0 meson while at intermediate p_T the u quark contributes significantly to the v_2 of D^0 meson. Using the smooth fit of discrete points of charm quark v_2 in panel (a) and those of light-flavor quarks in the corresponding centrality extracted from data of light-flavor hadrons [6], we predict in panel (b) the v_2 of D_s^+ meson, Λ_c^+ and Ξ_c^0 baryons. We see that in low p_T range v_2 of D_s^+ is close to those of Λ_c^+ and Ξ_c^0 and at intermediate p_T it is smaller than the latter. We also see that v_2 of Λ_c^+ is slightly smaller than that of Ξ_c^0 in the range $4 \lesssim p_T \lesssim 6$ GeV/c, which is the kinetic effect caused by the mass difference of u and s quarks in combination with charm quark.

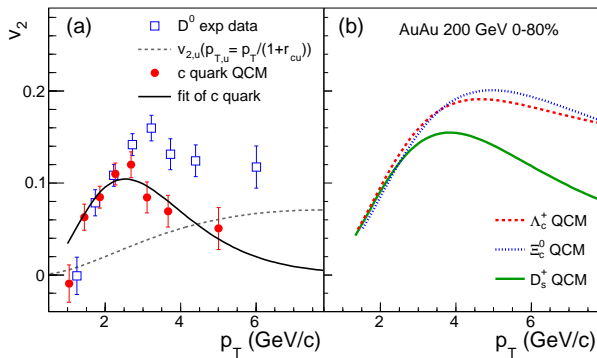


Figure 6. Panel (a) Charm quark v_2 extracted from midrapidity data of D^0 in Au+Au collisions at $\sqrt{s_{NN}} = 200$ GeV for 0-80% centrality [18], and (b) predictions for D_s^+ , Λ_c^+ and Ξ_c^0 in QCM.

VI. PROPERTIES FOR v_2 OF QUARK

In this section, we study the property for v_2 of up, strange and charm quarks obtained in previous sections. We focus on two main properties, i.e., flavor dependence

and the quark-antiquark split, which are discussed as follows.

A. compare v_2 of u , s and c quarks

As an example, in Fig. 7 (a), we present v_2 of up, strange and charm quarks in Pb+Pb collisions at $\sqrt{s_{NN}} = 5.02$ TeV for 30-50% centrality. We see that v_2 of up and strange quarks increase with p_T as $p_T \lesssim 1.5$ GeV/c and start to decrease at larger p_T . In particular, we see that v_2 of up quarks is higher than that of strange quarks in the range $p_T \lesssim 1.5$ GeV/c. For all the studied collisions energies and collision centralities, we always see this property. We have checked that if we replace p_T by $\sqrt{p_T^2 + m^2} - m$ in the horizontal axis, the split between up and strange quarks becomes small but does not disappear. v_2 of charm quarks at small $p_T \lesssim 2$ GeV/c has relatively large uncertainty and is roughly consistent with those of up and strange quarks. However, charm quark v_2 continues to increase and reaches the peak value about 0.13 at $p_T \approx 2.5$ GeV/c, which is obviously higher than those of light-flavor quarks (about 0.09) at $p_T \approx 1.5$ GeV/c.

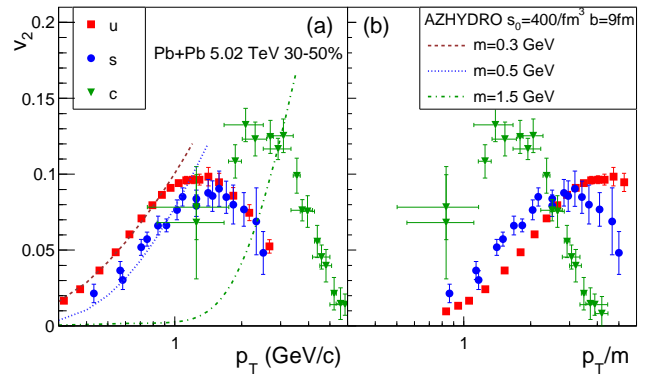


Figure 7. v_2 of up, strange and charm quarks in Pb+Pb collisions at $\sqrt{s_{NN}} = 5.02$ TeV for 30-50% centrality as a function of p_T (a) and of p_T/m (b). Lines are results of AZHYDRO code with initial entropy density $s_0 = 400/fm^3$, impact parameter $b = 9$ fm, and hadronization temperature $T = 0.165$ GeV.

For the increase of v_2 at small p_T for up and strange quarks, we can qualitatively understand it in general by the hydrodynamic evolution of quark gluon plasma (QGP) [39]. The v_2 for charm quarks is the result of the diffusion in QGP [40], which is related to many evolution dynamics such as the large collective flow, quench effects of the background medium and possible thermalization of charm quarks [40-46].

To understand the flavor difference of v_2 at small p_T , we apply the AZHYDRO code [39] for 2+1-dimensional hydrodynamics to study the qualitative behavior for v_2 of different quark flavors under thermal equilibrium and hydrodynamic flow velocity field. We set the criterion of

Cooper-Frye procedure by the fixed temperature. The temperature is taken as the hadronization temperature $T = 0.165$ GeV. We change the “freeze-out” particles as quarks in Cooper-Frye procedure and calculate the two-dimensional transverse momentum distributions of up, strange and charm quarks. The initial entropy density is set to be $s_0 = 400/fm^3$ and impact parameter is set to be $b = 9$ fm. The inelastic pp cross section is set to be 70 mb. Calculation results for v_2 of quarks are shown as lines in Fig. 7(a). We see AZHYDRO simulations, the dashed and dotted lines in Fig. 7(a), can well fit the extracted v_2 of up and strange quarks as $p_T \lesssim 1$ GeV/c. v_2 of charm quarks in the case of thermal equilibrium is also shown as the dot-dashed line. It is below the extracted charm v_2 at small p_T and intersects the latter at $p_T \approx 3$ GeV/c.

Because masses of up, strange and charm quarks are quite different, $p_T/m = \gamma v$ may be an alternative kinetic variable to reveal the regularity for v_2 of three quark flavors. In panel (b), we show quark v_2 as the function of p_T/m . Here, we see a clear property relating to quark mass: as $p_T/m \lesssim 2$ the quark with heavier mass has larger v_2 while the reverse behavior appears as $p_T/m \gtrsim 3$. We observe the same property in Au+Au collisions at $\sqrt{s_{NN}} = 200$ GeV for 0-80% centrality. This regularity of quark v_2 is interesting and is worthwhile to be studied in the future work.

B. v_2 split between quark and antiquark

STAR experiments observed the elliptic flow split between hadrons and their anti-hadrons at low collision energies [26]. In this paper, as shown in Fig. 2, we can apply the EVC model to successfully decompose v_2 of hadrons and their anti-hadrons into v_2 of quarks and antiquarks. Therefore, we can extract the v_2 split between quark and antiquark. Here, we take the data in Au+Au collisions at $\sqrt{s_{NN}} = 39$ GeV for 10-40% centrality as an example.

In Fig. 8 (a), we first present experimental data for the difference in v_2 between baryons and their anti-hadrons. We see that $v_{2,p} - v_{2,\bar{p}}$ show clearly positive values. $v_{2,\Lambda} - v_{2,\bar{\Lambda}}$ is also positive and is slightly smaller than $v_{2,p} - v_{2,\bar{p}}$. Data of $v_{2,\Xi} - v_{2,\bar{\Xi}}$ have relatively poor statistics and still show a positive tendency and smaller magnitude compared to $v_{2,p} - v_{2,\bar{p}}$ and $v_{2,\Lambda} - v_{2,\bar{\Lambda}}$. Data of $\Omega^- - \bar{\Omega}^+$ are not shown here because of bad statistics.

Using v_2 of quarks and that of antiquarks obtained in Fig. 2, we calculate $v_{2,u} - v_{2,\bar{u}}$ and show results in Fig. 8 (b). We obtain a good agreement between results obtained from $p - \bar{p}$ via Eq. (18) and those from $\Lambda - \bar{\Lambda}$ and $\Xi - \bar{\Xi}$ via Eq. (19). We see clearly the positive $v_{2,u} - v_{2,\bar{u}}$ with weak p_T dependence in the low p_T range ($p_T < 1$ GeV/c).

Results of $v_{2,s} - v_{2,\bar{s}}$ from $\Lambda - \bar{\Lambda}$ and $\Xi - \bar{\Xi}$ channel are shown in Fig. 8 (c). Because of large statistical uncertainties, the p_T dependence of $v_{2,s} - v_{2,\bar{s}}$ is not conclusive. For the overall sign of $v_{2,s} - v_{2,\bar{s}}$, we can roughly

estimate by averaging seven datum points and obtain 0.0002 ± 0.0029 , which might imply the equal v_2 for s and \bar{s} in Au+Au collisions at $\sqrt{s_{NN}} = 39$ GeV. Results of $v_{2,s} - v_{2,\bar{s}}$ at lower collision energies have poorer statistics and therefore we cannot draw further conclusion at present.

VII. SUMMARY AND OUTLOOK

We applied a quark combination model (QCM) with equal-velocity combination (EVC) approximation to study the elliptic flow (v_2) of identified hadrons in relativistic heavy-ion collisions at $\sqrt{s_{NN}} = 27 \sim 5020$ GeV. Under EVC, quarks contribute to the momentum of the formed hadron by the fraction proportional to their constituent masses. v_2 of hadron consisting of different constituent quarks is therefore the sum of v_2 of quarks with different transverse momenta. This is different from the number-of-constituent quark scaling (NCQ) operation in experimental study of hadronic v_2 [5–9].

Under EVC, we obtained simple formulas of reversely extracting v_2 of quarks and antiquarks from the experimental data of identified hadrons. By the combination of data for Λ and Ξ , we obtained v_2 of up/down quarks which is consistent with that from data of proton; we also obtained v_2 of strange quarks which is consistent with that from data of Ω . At RHIC energies, v_2 of strange quarks extracted from hyperons is also consistent with that from ϕ meson. This means that v_2 of these light-flavor hadrons have a common quark-level source at hadronization. At LHC energies, however, v_2 of strange quarks extracted from hyperons is somewhat lower than that from ϕ . This indicates the possible contribution of two-kaon coalescence to ϕ production at LHC energies.

Using results for v_2 of light flavor quarks, we further extracted v_2 of charm quarks from the data of D^0 meson in Pb+Pb collisions at $\sqrt{s_{NN}} = 5.02$ TeV and that in Au+Au collisions at 200 GeV. By comparing v_2 of charm quark and that of D^0 meson, we found that v_2 of D^0 meson at low p_T ($p_T \lesssim 3$ GeV/c) is dominated by that of charm quarks but at intermediate p_T ($3 \lesssim p_T \lesssim 8$ GeV/c) is significantly contributed by v_2 of light-flavor quarks. We predicted v_2 of D_s^+ meson, Λ_c^+ and Ξ_c^0 baryons. We found that v_2 of charmed baryons is significantly enhanced at intermediate p_T ($3 \lesssim p_T \lesssim 8$ GeV/c), compared to those of D mesons, which is due to the double contribution of light-flavor quarks.

We finally studied the properties of the extracted v_2 of quarks and antiquarks at hadronization. We first compared v_2 of up, strange and charm quarks. We found that v_2 of up quarks is always higher than that of strange quarks at low p_T ($p_T \lesssim 1$ GeV/c) at all studied collision energies. Such a mass hierarchy of quark v_2 can be reasonably understood by hydrodynamics. v_2 of charm quark at small p_T ($p_T \lesssim 1.5$ GeV/c) is roughly consistent with those of light-flavor quarks within the statistical uncertainty. However, differing from light-flavor

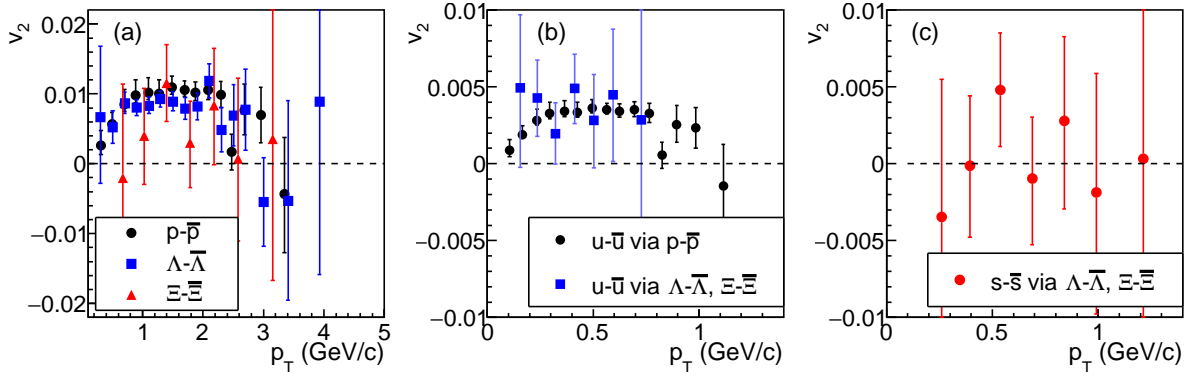


Figure 8. Panel(a): The difference in v_2 between hadrons and their anti-hadrons in Au+Au collisions at $\sqrt{s_{NN}} = 39$ GeV for 10-40% centrality. Data are from [26]; panel (b) the difference in v_2 between u and \bar{u} ; panel (c) that between s and \bar{s} .

quarks, v_2 of charm quarks continues to increase with p_T and reaches larger value at $p_T \approx 2.5$ GeV/c. Interestingly, by plotting quark v_2 as the function of transverse velocity p_T/m , we found a regularity relating to quark mass, i.e., as $p_T/m \lesssim 2$ the quark with heavier mass has larger v_2 while as $p_T/m \gtrsim 3$ reverse property holds. We further studied the difference in v_2 between quarks and antiquarks at low RHIC energies. We found that $v_{2,u} - v_{2,\bar{u}}$ extracted from hyperons and anti-hyperons coincides with that from proton and anti-proton. Results of $v_{2,s} - v_{2,\bar{s}}$ have large statistical uncertainties, and the average value of all datum points implies the symmetry in v_2 between strange quarks and strange antiquarks in Au+Au collisions at 39 GeV.

These results suggest that QCM with EVC is quite effective and self-consistent in understanding v_2 of hadrons in heavy-ion collisions. In addition, EVC mechanism provides an approximate method to obtain v_2 of quarks

and antiquarks at hadronization, by which we can obtain deeper insights into the information of partonic stage evolution in relativistic heavy-ion collisions. Finally, we emphasize that EVC is an effective but simplified mechanism. Studies on the application range and limitation of this mechanism are deserved with the help of more precise experimental data in the future.

VIII. ACKNOWLEDGMENTS

We gratefully acknowledge fruitful discussions with Z.T. Liang. This work is supported in part by the National Natural Science Foundation of China under Grant Nos. 11975011, Shandong Province Natural Science Foundation Grant Nos. ZR2019YQ06 and ZR2019MA053, and Higher Educational Youth Innovation Science and Technology Program of Shandong Province (2019KJJ010).

-
- [1] J.-Y. Ollitrault, *Phys. Rev.* **D46**, 229 (1992).
 - [2] H. Sorge, *Phys. Rev. Lett.* **82**, 2048 (1999), [arXiv:nucl-th/9812057 \[nucl-th\]](#).
 - [3] D. Teaney, J. Lauret, and E. V. Shuryak, *Phys. Rev. Lett.* **86**, 4783 (2001), [arXiv:nucl-th/0011058 \[nucl-th\]](#).
 - [4] P. Huovinen, P. F. Kolb, U. W. Heinz, P. V. Ruuskanen, and S. A. Voloshin, *Phys. Lett.* **B503**, 58 (2001), [arXiv:hep-ph/0101136 \[hep-ph\]](#).
 - [5] A. Adare *et al.* (PHENIX), *Phys. Rev. Lett.* **98**, 162301 (2007), [arXiv:nucl-ex/0608033 \[nucl-ex\]](#).
 - [6] L. Adamczyk *et al.* (STAR), *Phys. Rev. Lett.* **116**, 062301 (2016), [arXiv:1507.05247 \[nucl-ex\]](#).
 - [7] B. B. Abelev *et al.* (ALICE), *JHEP* **06**, 190 (2015), [arXiv:1405.4632 \[nucl-ex\]](#).
 - [8] S. Acharya *et al.* (ALICE), *JHEP* **09**, 006 (2018), [arXiv:1805.04390 \[nucl-ex\]](#).
 - [9] L. Adamczyk *et al.* (STAR), *Phys. Rev.* **C88**, 014902 (2013), [arXiv:1301.2348 \[nucl-ex\]](#).
 - [10] D. Molnar and S. A. Voloshin, *Phys. Rev. Lett.* **91**, 092301 (2003), [arXiv:nucl-th/0302014 \[nucl-th\]](#).
 - [11] R. Fries, B. Muller, C. Nonaka, and S. Bass, *Phys. Rev. C* **68**, 044902 (2003), [arXiv:nucl-th/0306027](#).
 - [12] R. Fries, B. Muller, C. Nonaka, and S. Bass, *Phys. Rev. Lett.* **90**, 202303 (2003), [arXiv:nucl-th/0301087](#).
 - [13] V. Greco, C. Ko, and P. Levai, *Phys. Rev. Lett.* **90**, 202302 (2003), [arXiv:nucl-th/0301093](#).
 - [14] P. F. Kolb, L.-W. Chen, V. Greco, and C. M. Ko, *Phys. Rev. C* **69**, 051901 (2004), [arXiv:nucl-th/0402049](#).
 - [15] V. Minissale, F. Scardina, and V. Greco, *Phys. Rev. C* **92**, 054904 (2015), [arXiv:1502.06213 \[nucl-th\]](#).

- [16] Y. Oh, C. M. Ko, S. H. Lee, and S. Yasui, *Phys. Rev. C* **79**, 044905 (2009), [arXiv:0901.1382 \[nucl-th\]](#).
- [17] S. Plumari, V. Minissale, S. K. Das, G. Coci, and V. Greco, *Eur. Phys. J. C* **78**, 348 (2018), [arXiv:1712.00730 \[hep-ph\]](#).
- [18] S. Singha (STAR), *Proceedings, 27th International Conference on Ultrarelativistic Nucleus-Nucleus Collisions (Quark Matter 2018): Venice, Italy, May 14-19, 2018*, *Nucl. Phys. A* **982**, 671 (2019), [arXiv:1807.04771 \[nucl-ex\]](#).
- [19] J. Song, X.-r. Gou, F.-l. Shao, and Z.-T. Liang, *Phys. Lett. B* **774**, 516 (2017), [arXiv:1707.03949 \[hep-ph\]](#).
- [20] J.-w. Zhang, H.-h. Li, F.-l. Shao, and J. Song, *Chin. Phys. C* **44**, 014101 (2020), [arXiv:1811.00975 \[hep-ph\]](#).
- [21] J. Song, F.-l. Shao, and Z.-t. Liang, *Phys. Rev. C* **102**, 014911 (2020), [arXiv:1911.01152 \[nucl-th\]](#).
- [22] X.-r. Gou, F.-l. Shao, R.-q. Wang, H.-h. Li, and J. Song, *Phys. Rev. D* **96**, 094010 (2017), [arXiv:1707.06906 \[hep-ph\]](#).
- [23] H.-H. Li, F.-L. Shao, J. Song, and R.-Q. Wang, *Phys. Rev. C* **97**, 064915 (2018), [arXiv:1712.08921 \[hep-ph\]](#).
- [24] J. Song, H.-h. Li, and F.-l. Shao, *Eur. Phys. J. C* **78**, 344 (2018), [arXiv:1801.09402 \[hep-ph\]](#).
- [25] J. Song, X.-f. Wang, H.-h. L. Li, R.-q. W. Wang, and F.-l. Shao, (2020), [arXiv:2007.14588 \[nucl-th\]](#).
- [26] L. Adamczyk *et al.* (STAR), *Phys. Rev. C* **93**, 014907 (2016), [arXiv:1509.08397 \[nucl-ex\]](#).
- [27] Y. Zhu (ALICE), *Proceedings, 39th International Conference on High Energy Physics (ICHEP2018): Seoul, Korea, July 4-11, 2018*, *PoS ICHEP2018*, 441 (2019).
- [28] B. I. Abelev *et al.* (STAR), *Phys. Rev. Lett.* **101**, 252301 (2008), [arXiv:0807.1518 \[nucl-ex\]](#).
- [29] B. Abelev *et al.* (ALICE), *Phys. Rev. Lett.* **111**, 232302 (2013), [arXiv:1306.4145 \[nucl-ex\]](#).
- [30] A. J. Baltz and C. Dover, *Phys. Rev. C* **53**, 362 (1996).
- [31] C. Alt *et al.* (NA49), *Phys. Rev. C* **78**, 044907 (2008), [arXiv:0806.1937 \[nucl-ex\]](#).
- [32] L.-X. Sun, R.-Q. Wang, J. Song, and F.-L. Shao, *Chin. Phys. C* **36**, 55 (2012), [arXiv:1105.0577 \[hep-ph\]](#).
- [33] Z.-w. Lin and D. Molnar, *Phys. Rev. C* **68**, 044901 (2003), [arXiv:nucl-th/0304045 \[nucl-th\]](#).
- [34] R.-Q. Wang, J. Song, F.-L. Shao, and Z.-T. Liang, *Phys. Rev. C* **101**, 054903 (2020), [arXiv:1911.00823 \[hep-ph\]](#).
- [35] S. Cao, G.-Y. Qin, and S. A. Bass, *Phys. Rev. C* **92**, 024907 (2015), [arXiv:1505.01413 \[nucl-th\]](#).
- [36] A. M. Sirunyan *et al.* (CMS), *Phys. Rev. Lett.* **120**, 202301 (2018), [arXiv:1708.03497 \[nucl-ex\]](#).
- [37] C. Collaboration (CMS), *Search for strong electromagnetic fields in PbPb collisions at 5.02 TeV via azimuthal anisotropy of D^0 and \bar{D}^0 mesons*, Tech. Rep. CMS-PAS-HIN-19-008 (2019).
- [38] L. Vermunt (ALICE), “Measurement of Λ_c^+ baryons and D_s^+ mesons in Pb-Pb collisions with ALICE,” (2019), [arXiv:1910.11738 \[nucl-ex\]](#).
- [39] P. F. Kolb, J. Sollfrank, and U. W. Heinz, *Phys. Rev. C* **62**, 054909 (2000), [arXiv:hep-ph/0006129 \[hep-ph\]](#).
- [40] R. Rapp and H. van Hees, in *Quark-gluon plasma 4* (2010) pp. 111–206, [arXiv:0903.1096 \[hep-ph\]](#).
- [41] B. Svetitsky, *Phys. Rev. D* **37**, 2484 (1988).
- [42] G. D. Moore and D. Teaney, *Phys. Rev. C* **71**, 064904 (2005), [arXiv:hep-ph/0412346 \[hep-ph\]](#).
- [43] H. van Hees and R. Rapp, *Phys. Rev. C* **71**, 034907 (2005), [arXiv:nucl-th/0412015 \[nucl-th\]](#).
- [44] M. He, R. J. Fries, and R. Rapp, *Phys. Rev. C* **86**, 014903 (2012), [arXiv:1106.6006 \[nucl-th\]](#).
- [45] S. Cao, G.-Y. Qin, and S. A. Bass, *Phys. Rev. C* **88**, 044907 (2013), [arXiv:1308.0617 \[nucl-th\]](#).
- [46] S. K. Das, F. Scardina, S. Plumari, and V. Greco, *Phys. Lett. B* **747**, 260 (2015), [arXiv:1502.03757 \[nucl-th\]](#).
- [47] S. Acharya *et al.* (ALICE), *Phys. Lett. B* **802**, 135225 (2020), [arXiv:1910.14419 \[nucl-ex\]](#).
- [48] J. Adam *et al.* (ALICE), *Phys. Rev. C* **95**, 064606 (2017), [arXiv:1702.00555 \[nucl-ex\]](#).
- [49] L. Adamczyk *et al.* (STAR), *Phys. Rev. C* **93**, 021903 (2016), [arXiv:1506.07605 \[nucl-ex\]](#).
- [50] B. I. Abelev *et al.* (STAR), *Phys. Rev. C* **79**, 064903 (2009), [arXiv:0809.4737 \[nucl-ex\]](#).
- [51] P. Kalinak (ALICE), *Proceedings, 2017 European Physical Society Conference on High Energy Physics (EPS-HEP 2017): Venice, Italy, July 5-12, 2017*, *PoS EPS-HEP2017*, 168 (2017).
- [52] S. Acharya *et al.* (ALICE), *Phys. Rev. C* **101**, 044907 (2020), [arXiv:1910.07678 \[nucl-ex\]](#).
- [53] B. Abelev *et al.* (ALICE), *Phys. Rev. C* **88**, 044910 (2013), [arXiv:1303.0737 \[hep-ex\]](#).
- [54] J. Adams *et al.* (STAR), *Phys. Rev. Lett.* **92**, 112301 (2004), [arXiv:nucl-ex/0310004 \[nucl-ex\]](#).
- [55] J. Adams *et al.* (STAR, STAR RICH), (2006), [arXiv:nucl-ex/0601042 \[nucl-ex\]](#).
- [56] L. Adamczyk *et al.* (STAR), *Phys. Rev. C* **96**, 044904 (2017), [arXiv:1701.07065 \[nucl-ex\]](#).
- [57] J. Adam *et al.* (STAR), *Phys. Rev. C* **102**, 034909 (2020), [arXiv:1906.03732 \[nucl-ex\]](#).
- [58] B. B. Abelev *et al.* (ALICE), *Phys. Rev. Lett.* **111**, 222301 (2013), [arXiv:1307.5530 \[nucl-ex\]](#).
- [59] B. B. Abelev *et al.* (ALICE), *Phys. Lett. B* **728**, 216 (2014), [Erratum: *Phys. Lett. B* 734, 409 (2014)], [arXiv:1307.5543 \[nucl-ex\]](#).

Appendix A: v_2 of pion and kaon

Because the masses of pion and kaon are small, the production of pion and kaon is not suitably described by the direct combination of constituent quarks and antiquarks. To reconcile the mass mismatch, we adopt a naive treatment [22] which provides the good description for the p_T distribution of pions and that of kaons. We consider the processes such as $u + \bar{d} \rightarrow \pi + X$ for pion production and $u + \bar{s} \rightarrow K + X$ for kaon production. Here X is some soft degrees of freedom. For simplicity, we identify X as soft pions. As an example, using the extracted v_2 of u and s quarks in Au+Au collisions at $\sqrt{s_{NN}} = 200$ GeV for 30-80% centrality, we calculate v_2 of the directly-produced pions and kaons by above processes and then consider the decay contribution of other hadrons. We show results as solid lines, marked as “final π/K QCM”, in Fig. 9 and compare with experimental data [6]. We see that v_2 of pion and kaon in the low p_T range ($p_T \lesssim 2$ GeV/c) can be described by v_2 of quarks that is extracted from baryons and ϕ .

As a contrast, we also calculate v_2 of pions and that of kaons by direct EVC formulas, i.e., $v_{2,\pi}(p_T) = 2v_{2,u}(p_T/2)$ and $v_{2,K}(p_T) = v_{2,u}(\frac{1}{1+r}p_T) + v_{2,s}(\frac{r}{1+r}p_T)$. We present results as dashed lines in Fig. 9, marked as “direct π/K QCM”. Comparing to solid lines, we see the important effect of extra X in pion and kaon production and that of resonance decays.

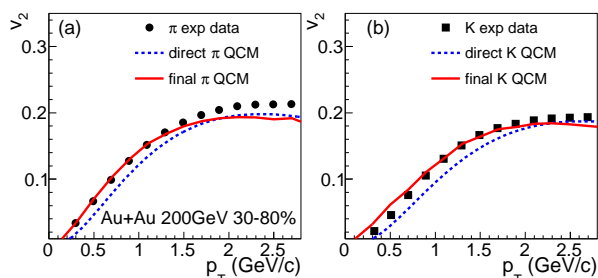


Figure 9. v_2 of pion and kaon in Au+Au collisions at $\sqrt{s_{NN}} = 200$ GeV for 30-80% centrality. Symbols are experimental data [6]. Dashed lines are results of v_2 directly applying EVC formulas. Solid lines are results of $u + \bar{d}/\bar{s} \rightarrow \pi/K + X$ process after considering the decay contribution of other hadrons.

Appendix B: the influence of two-kaon coalescence on p_T spectrum of ϕ

Starting from Eqs. (1) and (2), the p_T distributions of Ω and ϕ under equal-velocity combination have

$$f_{\Omega}(p_T) = \kappa_{\Omega} f_s^3(p_T/3), \quad (B1)$$

$$f_{\phi}(p_T) = \kappa_{\phi} f_s^2(p_T/2) \quad (B2)$$

from which we get a quark number scaling property

$$f_{\Omega}^{1/3}(3p_T) = \kappa_{\phi,\Omega} f_{\phi}^{1/2}(2p_T), \quad (B3)$$

where $\kappa_{\phi,\Omega} = \kappa_{\Omega}^{1/3}/\kappa_{\phi}^{1/2}$ is independent of p_T . We take $f_s(p_T) = f_{\bar{s}}(p_T)$ at LHC energies.

As the discussion of ϕ elliptic flow at LHC energies in Sec. IV, the coalescence of two kaons may be another contribution to ϕ production. The p_T spectrum of ϕ by the coalescence of two charged kaons with equal velocity is

$$f_{\phi,KK}(p_T) \propto f_{K^+}(p_T/2) f_{K^-}(p_T/2) \quad (B4)$$

or by that of two neutral kaons is

$$f_{\phi,KK}(p_T) \propto f_{K^0}(p_T/2) f_{\bar{K}^0}(p_T/2) \propto [f_{K_s^0}(p_T/2)]^2. \quad (B5)$$

We use experimental data of K^{\pm} and K_s^0 in central heavy-ion collisions to calculate results of two-kaon coalescence by Eqs. (B4) and (B5) and compare calculation results with experimental data of ϕ in the same collision centrality. Fig. 10 shows results and comparisons at four collision energies. The centrality at each collision energy is selected by the condition that experimental data of K^{\pm} , K_s^0 and ϕ are all available. We see that the spectra of two-kaon coalescence are almost parallel to those of ϕ for $p_{T,\phi} \lesssim 4$ GeV/c. This indicates that two-kaon coalescence does not change the shape of ϕ distribution in this p_T range. Therefore, it also does not break the quark number scaling property Eq. (B3) in the range $p_{T,\phi} \lesssim 4$ GeV/c, equivalently, in the range $p_{T,s} \lesssim 2$ GeV/c dominated by soft or thermal strange quarks.

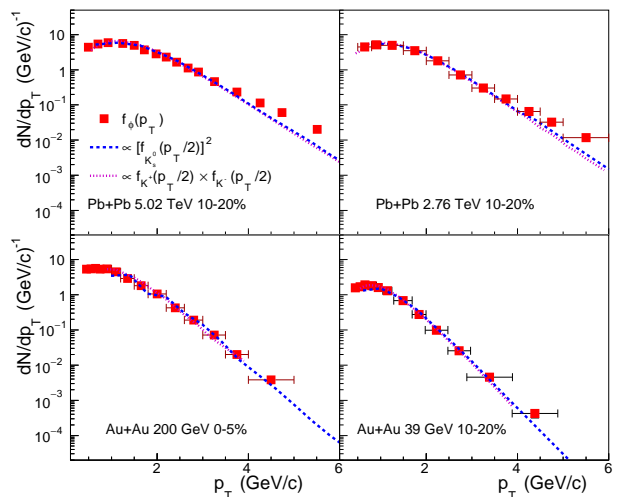


Figure 10. The p_T spectra by the coalescence of two kaons with equal velocity, which are compared with those of ϕ . Data of ϕ are taken from Refs. [47–50] and those of kaons used to calculate two-kaon coalescence are taken from Refs. [51–58].

In the range $p_T \gtrsim 4$ GeV/c, see top panels in Fig. 10, the spectra of two-kaon coalescence are steeper than those of ϕ to a certain extent. Therefore including this contribution will make ϕ spectrum softer than that formed purely by the strange quark combination. Here, we take a simple case as an illustration, i.e., 80% of final-state ϕ comes from the direct strange quark combination and the remaining 20% comes from two-kaon coalescence. Fig. 11 shows our calculations and the comparison with data of ϕ in Pb+Pb collisions at $\sqrt{s_{NN}} = 2.76$ TeV for 10-20% centrality [48]. Firstly, we present the results of pure strange quark combination at hadronization, the solid squares, which can be calculated using the data of Ω [59] by the scaling property Eq. (B3),

$$f_{\phi, s\bar{s}}(p_T) = \kappa_{\phi, \Omega}^{-2} f_{\Omega}^{2/3}(3p_T/2). \quad (\text{B6})$$

We see that they are in good agreement with data of ϕ for $p_T \lesssim 4$ GeV/c and the last point at $p_T = 4.3$ GeV/c is higher than the ϕ datum to a certain extent. Then, we consider the contribution of two-kaon coalescence and results are shown as up-triangles. Data of kaons are taken from Ref. [53]. We see that the results for $p_T \lesssim 3.5$ GeV/c are almost unchanged compared with those of

pure strange quark combination. The last two points at $p_T = 3.7$ and 4.3 GeV/c are decreased to a certain extent and are closer to the data of ϕ .

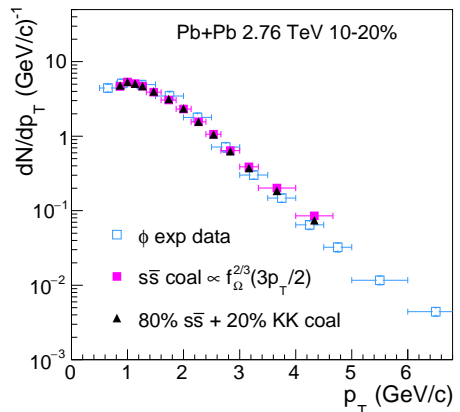


Figure 11. The p_T spectrum of ϕ calculated by pure $s\bar{s}$ combination and that by mixture of $s\bar{s}$ combination and KK coalescence in Pb+Pb collisions at $\sqrt{s_{NN}} = 2.76$ TeV for 10-20% centrality. Results are compared with data of ϕ [48].